Supplementary Information

H/F Substitution Achieves High Piezoelectricity in Enantiomeric Molecular Crystals

Wei-Xin Mao,[a] Long-Xing Zhou,[a] Xin Deng,[a] Jin-Fei Lan,[a] Xian-Jiang Song[a]* and Han-Yue Zhang[b]*

Experimental

Synthesis of *R*、*S and Rac*-H. *R*-1-(4-methoxyphenyl) ethylamine (0.756 g, 5 mmol) and an equivalent amount of benzoic acid were dissolved thoroughly in 20 mL of methanol, respectively. After mixing the two solutions, 10 mL of methanol was added. Then, the solution was stirred until clear. The *R*-H crystal was obtained by slow evaporation at room temperature. By replacing *R*-1-(4-methoxyphenyl) ethylamine with the corresponding amine, the crystals of *S*-H and *Rac*-H were grown in the same way.

Synthesis of *R*、*S and Rac*-F. *R*-1-(4-methoxyphenyl) ethylamine (0.756 g, 5 mmol) and an equivalent amount of p-fluorobenzoic acid were dissolved thoroughly in 20 mL of methanol, respectively. After mixing the two solutions, 10 mL of methanol was added. Then, the solution was stirred until clear. The *R*-F crystal was obtained by slow evaporation at room temperature. By replacing *R*-1-(4-methoxyphenyl) ethylamine with the corresponding amine, the crystals of *S*-F and *Rac*-F were grown in the same way.

Single-crystal X-ray crystallography (XRD). Variable-temperature X-ray single-crystal diffractions were performed on Rigaku Oxford diffractometer with Cu-Kα radiation (λ = 1.54184 Å). The SHELX program package on the Olex2 program solved the structure data and structure refinement. The data collection and structure refinement of these crystals are summarized in Table S1-S2. (CCDC number: 2366876-2366883).

Powder X-ray diffraction (PXRD). Variable-temperature powder X-ray diffraction (PXRD) data were collected by using a Rigaku D/MAX 2000 PC X-ray diffraction system with Cu Kα radiation in the 2θ range of 5-40° with a step size of 0.02°.

Differential Scanning Calorimetry (DSC), Second Harmonic Generation (SHG) and thermogravimetric Analyses (TGA) Measurements. DSC measurements were recorded on a NETZSCH DSC 200F3 instrument by heating and cooling crystalline samples with a rate of 10 $K \cdot min^{-1}$ under in aluminum crucibles at nitrogen atmosphere. SHG measurements were carried out on FLS 920, Edinburgh Instruments using an unexpanded laser beam with low divergence (pulsed Nd: YAG at a wavelength of 1064 nm). The laser is Vibrant 355 II, OPOTEK. TGA from 300 to 800 K were carried out

by using a PerkinElmer TGA 8000.

The complex dielectric permittivity. For the dielectric measurements, the polycrystalline sample was grounded into powder and pressed into a thin plate. Then we deposited the conductive silver glue on the both top and bottom plate surfaces as the electrodes of the sample sheet. Next, we stuck the copper wire on it by using silver conducting glue for connection with the six-hole socket, forming a capacitor. The dielectric measurement was carried out on a Tonghui 2828 impedance analyzer at 1 MHz.

Nanoindentation method. Nanoindentation characterizations were performed on a nanoindenter (Bruker, Hysitron TI Premier). The testing probe adopted was a standard diamond Berkovich probe with radius of curvature of 150 nm. Samples were adhered to stainless iron disk which could be fixed firmly onto the sample stage of the testing instrument by static magnetic attraction. For each sample, at least two different positions were indented with distance of 10 μm to avoid interference and the results were averaged out from them. The elastic modulus and hardness were obtained through Oliver-Pharr method provided by the instrument.

Raman spectroscopy. The Raman spectra were measured by the Raman spectrometer (Horiba, LabRAM HR Evolution) with a reflection method. The excitation laser was 633 nm. A 50× microscope objective was used to focus the excitation on the samples. The spectra were dispersed by a 600-groove per millimeter diffraction grating and accumulated 3 times with an exposing time of 2 s. Temperature-dependent Raman measurements were achieved by equipped with a temperature controller (Linkam).

The temperature-dependent Raman spectroscopy measurement on *R*-F crystal was carried out to further verify their thermodynamic phase transition (Figure S12a-b). As the temperature increases from 290 K to 340 K, the Raman peak center at 3081 cm^{-1} (C-H stretching) shifts and gradually merges. Similarly, as the temperature drops back to 290 K, the single peak at 3074 cm^{-1} can also return to the original shoulder peak form, which is basically consistent with the DSC measurement result. This indicates that the temperature-induced phase transition is completely reversible.

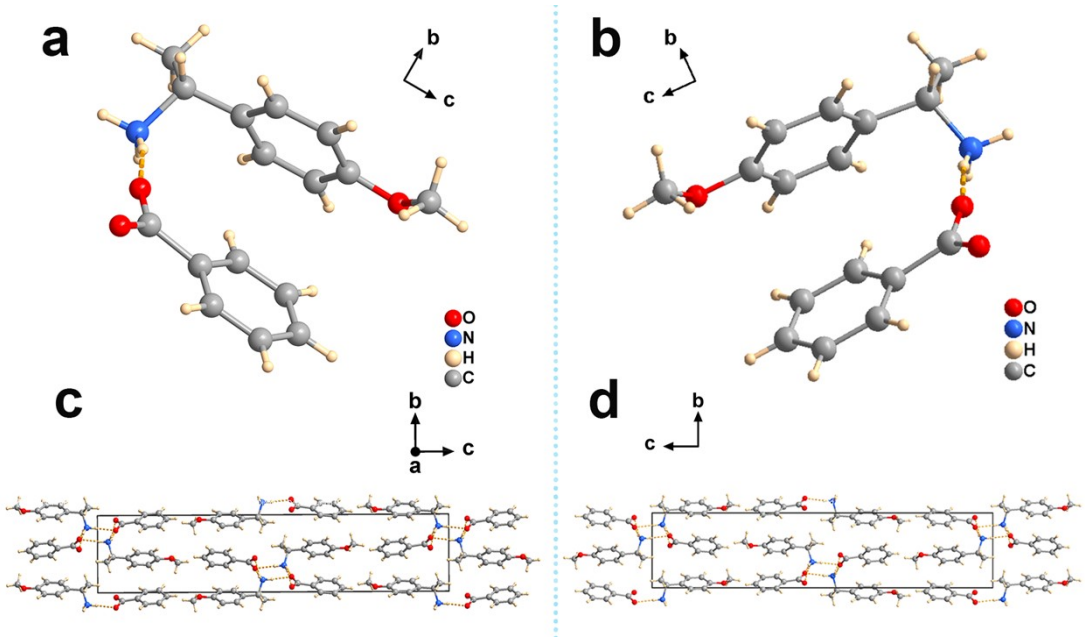

Figure S1. Mirror-image relationship of *R*-H and *S*-H at 299 K. The basic units of (a) *R*-H and (b) *S*-H. Packing views of (c) *R*-H and (d) *S*-H along the *a*-axis at 299 K. The blue dashed line denotes a mirror plane.

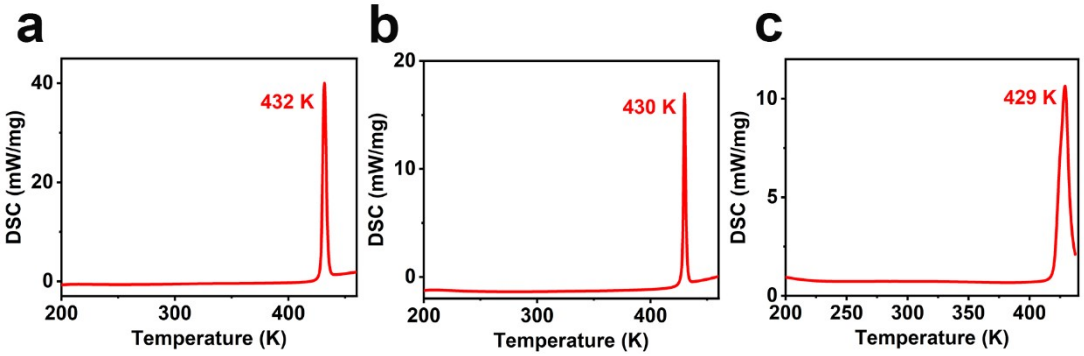

Figure S2. DSC curves of *R*-H (a), *S*-H (b), and *Rac*-H (c).

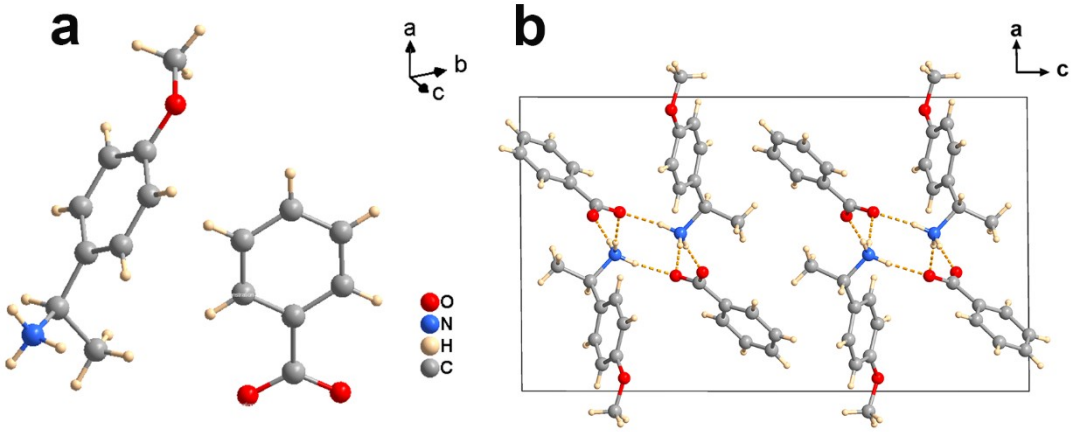

Figure S3. The basic asymmetric unit of the *Rac*-H crystal (a) and packing view along the *b*-axis at 299 K (b).

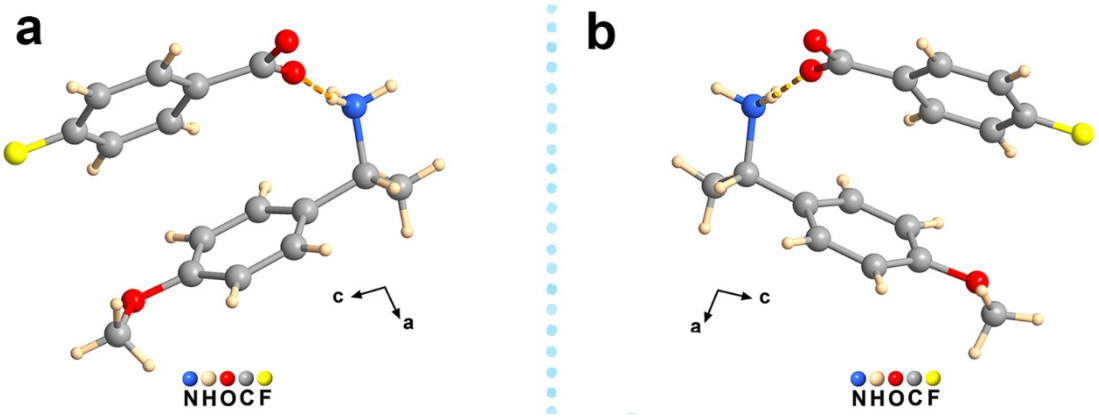

Figure S4. The basic asymmetric unit of the *R*-F crystal (a) and *S*-F crystal view along the *b*-axis at 340 K (b).

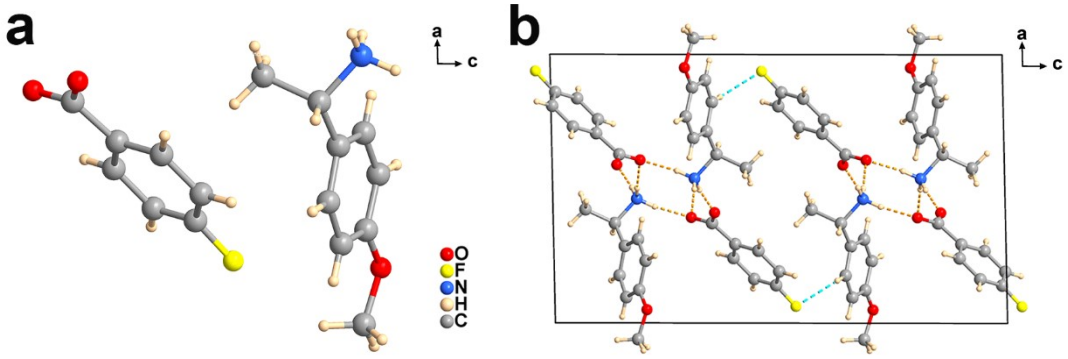

Figure S5. The basic asymmetric unit of the *Rac*-F crystal (a) and packing view along the *b*-axis at 300 K (b).

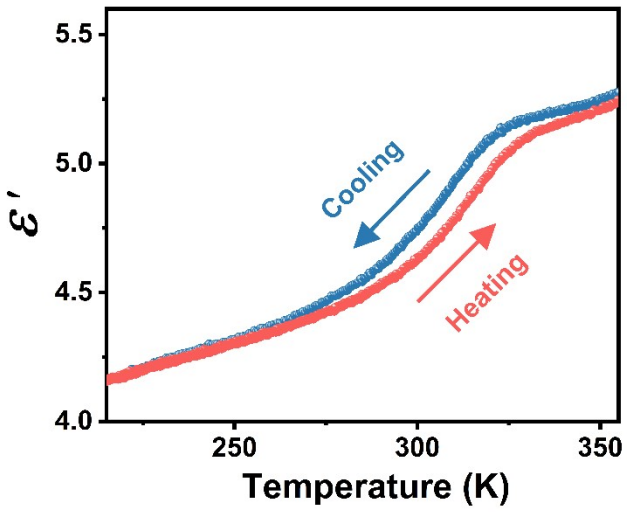

Figure S6. Temperature-dependent ε' at 1 MHz of *S*-F.

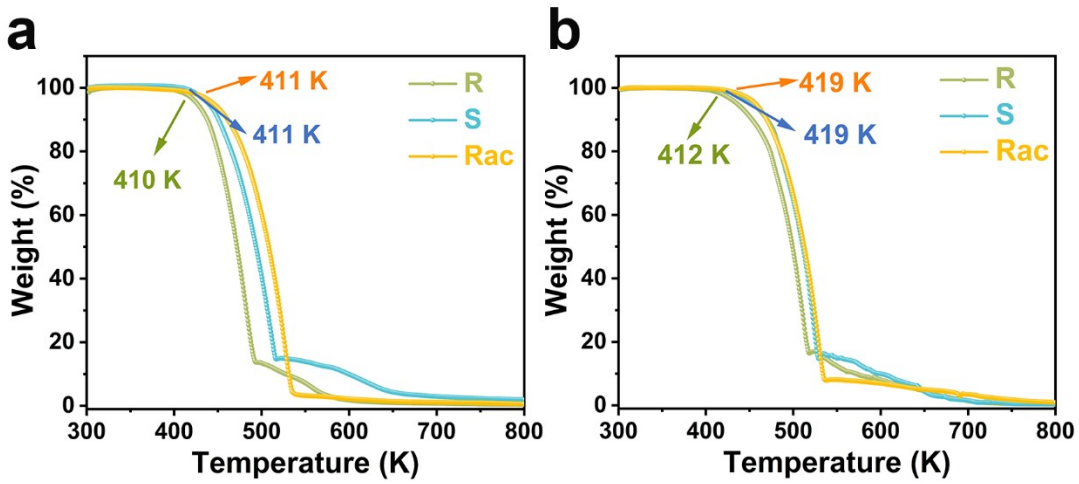

Figure S7. TGA curves (a) of *R*-H, *S*-H, and *Rac*-H. TGA curves (b) of *R*-F, *S*-F, and *Rac*-F.

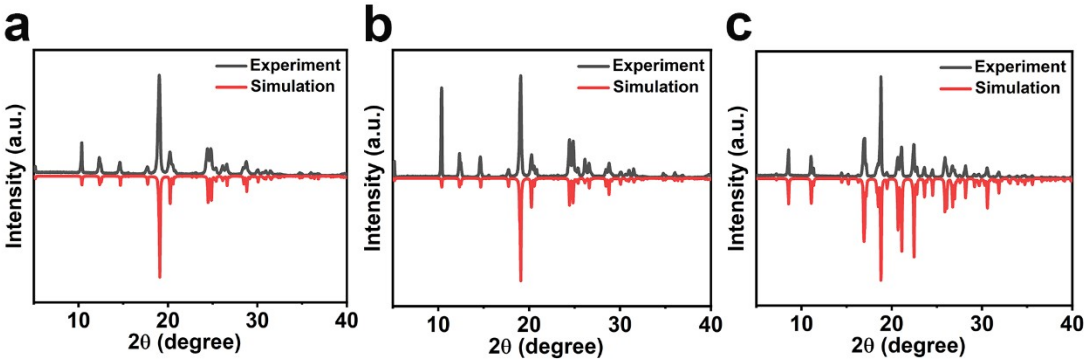

Figure S8. The measured and simulated PXRD patterns of *R*-F (a), *S*-F (b), and *Rac*-F (c).

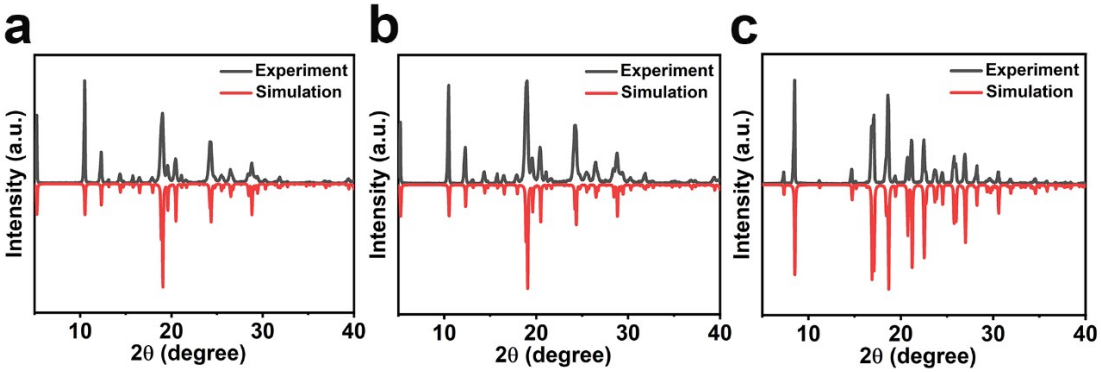

Figure S9. The measured and simulated PXRD patterns of *R*-H (a), *S*-H (b), and *Rac*-H (c).

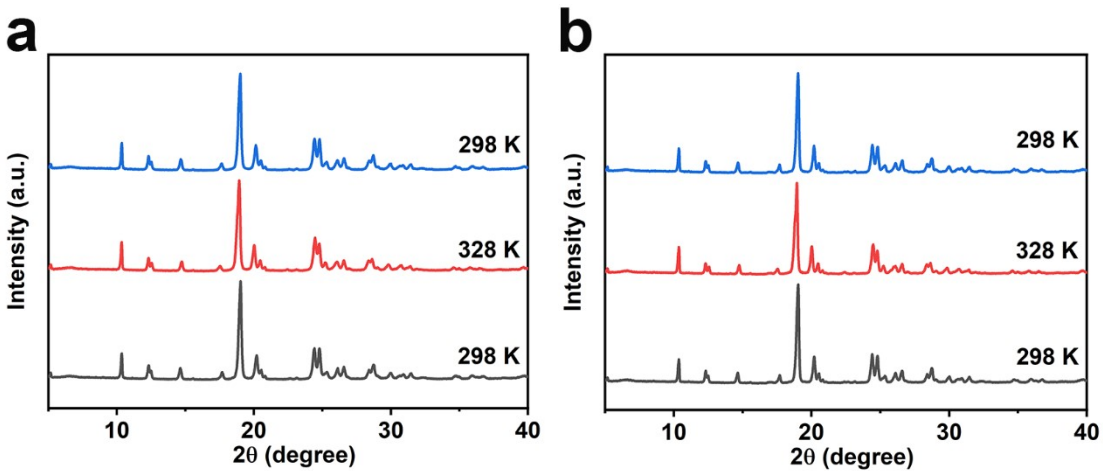

Figure S10. VT-PXRD of *R*-F (a) and *S*-F (b).

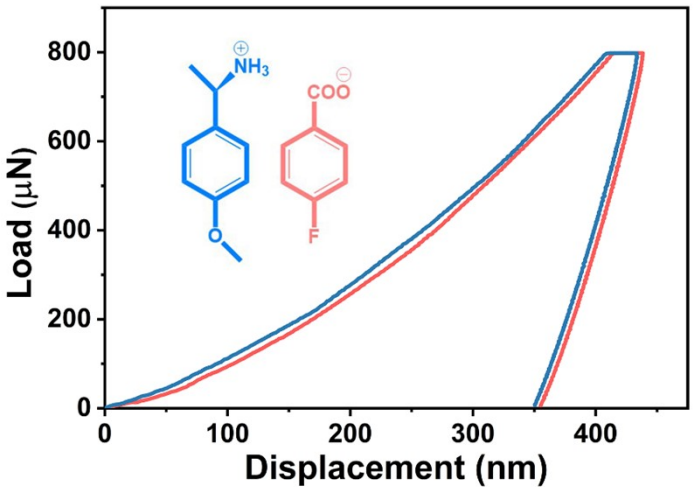

Figure S11. Typical load-displacement curves of the single crystals of *R*-F measured via a Berkovich indenter.

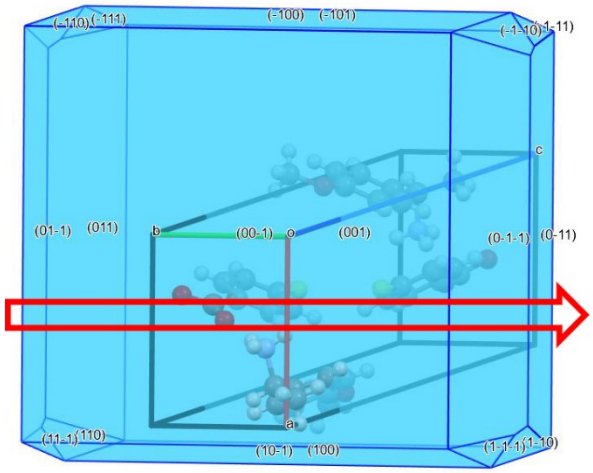

Figure S12. The simulated morphology of the crystal *R*-F. The red arrows indicate the directions for the quasi-static piezoelectric measurement.

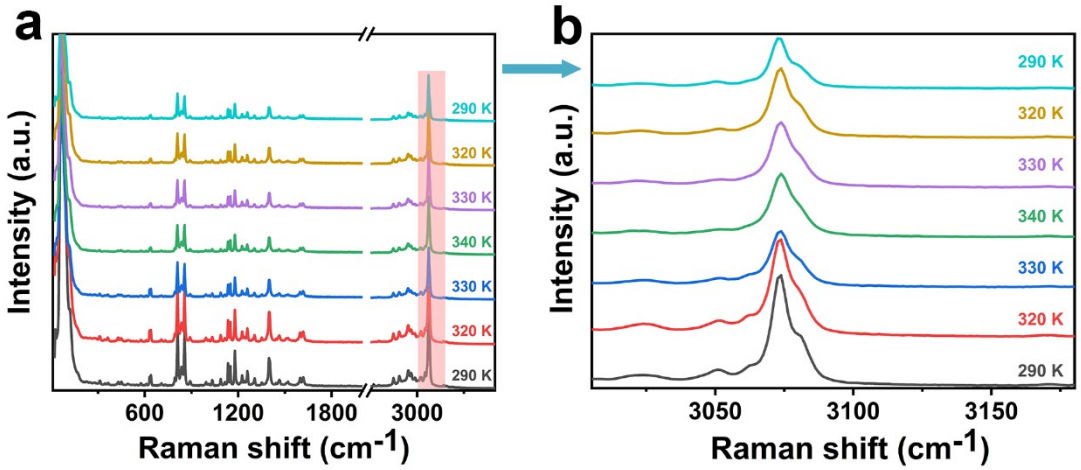

Figure S13. Temperature-dependent Raman spectra show thermal-induced phase transitions (a) and partially enlarged detail (b) (marked with pink dashed boxes).

Table S1. Crystal data and structure refinement for *R/S*-F at 296 K and 340 K.

Compound	***R*-F**	***R*-F**	***S*-F**	***S*-F**
Formula	$C_{16}H_{18}FNO_3$	$C_{16}H_{18}FNO_3$	$C_{16}H_{18}FNO_3$	$C_{16}H_{18}FNO_3$
Temperature	296 K	340 K	296 K	340 K
Formula weight	291.31	291.31	291.31	291.31
Crystal system	*monoclinic*	*monoclinic*	*monoclinic*	*monoclinic*
Space group	$P2_1$	$P2_1$	$P2_1$	$P2_1$
a/Å	7.2717(9)	7.2750(8)	7.2820(2)	7.2717(9)
b/Å	6.1735(9)	6.2945(7)	6.1726(2)	6.3005(13)
c/Å	17.314(2)	17.3045(18)	17.3070(5)	17.295(2)
α/°	90	90	90	90
β/°	100.127(12)	99.161(10)	100.162(2)	99.245(12)
γ/°	90	90	90	90
V/Å^3	765.17(18)	782.31(15)	765.73 (4)	782.1(2)
Z	2	2	2	2
ρ/g.cm^3	1.264	1.237	1.263	1.237
$R_1[I >= 2\sigma(I)]$	0.0780	0.0755	0.0600	0.0884
$wR_2[I >= 2\sigma(I)]$	0.2213	0.2082	0.1807	0.2835

GOF	1.142	1.062	1.082	1.178

Table S2. Crystal data and structure refinement for *R/S*-H and *Rac*-H/F at 300 K.

Compound	***R*-H**	***S*-H**	***Rac*-H**	***Rac*-F**
Formula	$C_{16}H_{19}NO_3$	$C_{16}H_{19}NO_3$	$C_{16}H_{19}NO_3$	$C_{16}H_{18}FNO_3$
Temperature	300 K	300 K	300 K	300 K
Formula weight	273.32	273.32	273.32	291.31
Crystal system	*orthorhombic*	*orthorhombic*	*monoclinic*	*monoclinic*
Space group	$P2_12_12_1$	$P2_12_12_1$	$P2_1/c$	$P2_1/c$
a/Å	6.1092(2)	6.1046(2)	12.0189(3)	12.2351(3)
b/Å	7.3483(3)	7.3469(2)	6.0835(2)	6.07500(10)
c/Å	33.6266(12)	33.6375(9)	20.7340(6)	20.6390(4)
α/°	90	90	90	90
β/°	90	90	90.471(3)	91.293(2)
γ/°	90	90	90	90
V/Å^3	1509.57(10)	1508.64(8)	1515.96(8)	1533.67(5)
Z	4	4	4	4
ρ/g.cm^3	1.203	1.203	1.198	1.262
$R_1[I >= 2\sigma(I)]$	0.0459	0.0496	0.0419	0.0388
$wR_2[I >= 2\sigma(I)]$	0.1477	0.1420	0.1175	0.1070
GOF	1.102	1.050	1.050	1.067

Hydrogen bond lengths (Å) and angles (º) for *R*/*S*-F at 296 K and 340 K, *R*/*S*-H, *Rac*-H/F at 300 K, respectively.

Table S3. Hydrogen Bonds for *R*-F-296 K.

D	H	A	d(D-H)/Å	d(H-A)/Å	d(D-A)/Å	D-H-A/°
N1	H1A	O2[1]	0.89	2.01	2.880(6)	166.3
N1	H1B	O2	0.89	1.88	2.766(7)	174.2
N1	H1C	O3[2]	0.89	1.92	2.781(6)	162.8

C1	H1D	F1[4]	0.96	2.64	3.412(12)	138.2

[1]1-X,-1/2+Y,-Z; [2]+X,-1+Y,+Z; [3]1+X,-1+Y,+Z; [4]1+X,+Y,+Z; [5]2-X,-1/2+Y,1-Z; [6]2-X,1/2+Y,1-Z

Table S4. Hydrogen Bonds for *R*-F-340 K.

D	H	A	d(D-H)/Å	d(H-A)/Å	d(D-A)/Å	D-H-A/°
N1	H1A	O3[1]	0.89	2.23	3.012(6)	146.1
N1	H1A	O2[1]	0.89	2.18	3.006(7)	153.8
N1	H1C	O3[2]	0.89	1.92	2.784(7)	164.2
N1	H1B	O2	0.89	1.86	2.739(7)	171.9
C1	H1E	F1[3]	0.96	2.70	3.467(15)	136.8

[1]1-X,-1/2+Y,-Z; [2]+X,-1+Y,+Z; [3]1+X,+Y,+Z; [4]2-X,1/2+Y,1-Z

Table S5. Hydrogen Bonds for *S*-F-296 K.

D	H	A	d(D-H)/Å	d(H-A)/Å	d(D-A)/Å	D-H-A/°
N1	H1A	O2[1]	0.89	2.01	2.874(4)	163.5
N1	H1C	O2	0.89	1.88	2.768(5)	174.5
N1	H1B	O3[2]	0.89	1.92	2.788(5)	163.1
C9	H9A	F1[4]	0.96	2.65	3.429(9)	139.0

[1]1-X,1/2+Y,-Z; [2]+X,1+Y,+Z; [3]1+X,1+Y,+Z; [4]1+X,+Y,+Z; [5]2-X,1/2+Y,1-Z; [6]2-X,-1/2+Y,1-Z

Table S6. Hydrogen Bonds for *S*-F-340 K.

D	H	A	d(D-H)/Å	d(H-A)/Å	d(D-A)/Å	D-H-A/°
N1	H1A	O3[1]	0.89	2.23	2.982(9)	141.5
N1	H1A	O2[1]	0.89	2.16	3.013(10)	159.4
N1	H1B	O3[2]	0.89	1.95	2.815(11)	164.0
N1	H1C	O2	0.89	1.84	2.721(13)	172.9
C9	H9A	F1[3]	0.96	2.70	3.455(19)	135.5

[1]1-X,1/2+Y,-Z; [2]+X,1+Y,+Z; [3]1+X,+Y,+Z; [4]2-X,-1/2+Y,1-Z

Table S7. Hydrogen Bonds for *Rac*-F-300 K.

D	H	A	d(D-H)/Å	d(H-A)/Å	d(D-A)/Å	D-H-A/°
N1	H1A	O1[1]	0.89	1.80	2.6834(15)	171.6
N1	H1B	O2[2]	0.89	1.92	2.8035(16)	170.6

N1	H1C	O2[3]	0.89	1.90	2.7682(14)	164.8
C4	H4	F1[6]	0.93	2.52	3.3428(18)	147.0

[1]1-X,1-Y,1-Z; [2]1-X,-Y,1-Z; [3]+X,1/2-Y,1/2+Z; [4]+X,-1/2-Y,1/2+Z; [5]-X,1/2+Y,3/2-Z; [6]+X,1+Y,+Z

Table S8. Hydrogen Bonds for *R*-H-300 K.

D	H	A	d(D-H)/Å	d(H-A)/Å	d(D-A)/Å	D-H-A/°
N1	H1A	O2[1]	0.89	1.98	2.843(3)	162.5
N1	H1B	O2	0.89	1.89	2.766(3)	170.1
N1	H1C	O3[2]	0.89	1.93	2.792(4)	161.6

[1]1/2+X,1/2-Y,1-Z; [2]1+X,+Y,+Z; [3]1+X,1+Y,+Z

Table S9. Hydrogen Bonds for *S*-H-300 K.

D	H	A	d(D-H)/Å	d(H-A)/Å	d(D-A)/Å	D-H-A/°
N1	H1A	O1[1]	0.89	1.98	2.842(3)	162.2
N1	H1B	O2[2]	0.89	1.93	2.789(4)	161.3
N1	H1C	O1	0.89	1.89	2.768(3)	169.9

[1]-1/2+X,1/2-Y,1-Z; [2]-1+X,+Y,+Z

Table S10. Hydrogen Bonds for *Rac*-H-300 K.

D	H	A	d(D-H)/Å	d(H-A)/Å	d(D-A)/Å	D-H-A/°
N1	H1A	O1[1]	0.89	1.90	2.7662(14)	165.5
N1	H1B	O1[2]	0.89	1.92	2.8033(16)	171.9
N1	H1C	O2[3]	0.89	1.81	2.6931(16)	171.6

[1]+X,3/2-Y,-1/2+Z; [2]1-X,2-Y,1-Z; [3]1-X,1-Y,1-Z; [4]2-X,-1/2+Y,1/2-Z; [5]+X,-1+Y,+Z; [6]+X,5/2-Y,-1/2+Z